Palaeontologia Electronica
palaeo-electronica.org

Differentiating convergent pathologies in turtle shells using computed tomographic scanning of modern and fossil bone

Stephanie K. Drumheller, Hannah Maddox, Michelle R. Stocker, and Christopher R. Noto

ABSTRACT

Patterns of bone damage can provide insights into the paleobiology and paleoecology of extinct groups, but accessing these data relies on accurate identifications. Among turtles, there are persistent concerns that shell disease and vertebrate feeding traces are confoundingly convergent. Though extreme cases of shell disease and more penetrative bite marks are more easily differentiated, more subtle examples of each can exhibit very similar morphologies. Given the different ways these two types of bone damage form, one through compression and impact damage and the other through immune system response to foreign bodies or infection, internal textures of the bone should provide helpful data to differentiate these convergent pathologies. Here we use microcomputed tomographic (μCT) scanning to visualize internal bone damage in known examples of modern bite marks and shell disease in *Trachemys* carapace and plastron elements. Observed patterns are then compared to fossil examples of putative bite marks and shell disease from Cenomanian turtle shell fragments from the Woodbine Group of north-central Texas, U.S.A. Modern and fossil examples of shell disease exhibit an irregular, bubble-like texture in cross section that erodes away the subsurface below the surficial marks, whereas the bite marks exhibited more regular U- or V-shaped indentations in cross section, underlain by fractured, compressed bone. Our study demonstrates that while different bone modifying processes can produce similar, surficial patterns, internal damage patterns can provide an alternate method for differentiating them. This suggests that internal visualization techniques have been underutilized when attempting to untangle surficial modifications affected by equifinality.

Stephanie K. Drumheller. Department of Earth and Planetary Sciences, University of Tennessee, Knoxville, Tennessee 37996, USA. Corresponding author. sdrumhel@utk.edu
Hannah Maddox. Department of Earth and Planetary Sciences, University of Tennessee, Knoxville, Tennessee 37996, USA. hmaddox2@vols.utk.edu

Final citation: Drumheller, Stephanie K., Maddox, Hannah, Stocker, Michelle R., and Noto, Christopher R. 2023. Differentiating convergent pathologies in turtle shells using computed tomographic scanning of modern and fossil bone. Palaeontologia Electronica, 26(2):a15.
https://doi.org/10.26879/1230
palaeo-electronica.org/content/2023/3830-bite-marks-and-shell-disease-comparison

Michelle R. Stocker. Department of Geosciences, Virginia Tech, Blacksburg, VA, 24061, USA. stockerm@vt.edu
Christopher R. Noto. Department of Biological Sciences, University of Wisconsin – Parkside, Kenosha, Wisconsin, 53141, USA. noto@uwp.edu

Keywords: taphonomy; paleopathology; Crocodylia; Testudines; Cenomanian; Cretaceous

Submission: 1 July 2022. Acceptance: 11 April 2023.

INTRODUCTION

Numerous processes can damage or modify bone, both during the life of an animal (e.g., osteomyelitis, fracture healing; Katsura, 2004; Mackness et al., 2010; Zonneveld et al., 2015; Hamm et al., 2020) and throughout the postmortem interval (e.g., scavenging, desiccation; Behrensmeyer et al., 1986; Augustin et al., 2019; Drumheller et al., 2020; McHugh et al., 2020). In the fossil record, these alterations can provide rare insights into the paleoecology and paleobiology of the affected groups (e.g., Tanke and Currie, 1998; Rega et al., 2012; Drumheller et al., 2014). However, these interpretations are predicated on the ability of paleopathologists, ichnologists, and taphonomists to differentiate those traces and pathologies. This can be compounded by convergence between bone modifying processes, i.e., equifinality.

Among fossilized turtles, there are persistent concerns regarding how to differentiate vertebrate bite marks, a type of crushing or impact trauma caused by teeth, and shell disease, a suite of structures formed when microorganisms or foreign bodies are introduced between the carapace or plastron and the overlying keratinous scutes, resulting in pitting or scoring of the underlying bone (e.g., Hunt, 1957; Lovich et al., 1996; Garner et al., 1997; Jacobson, 2007). Even in modern populations, shell disease is a poorly characterized, catch-all term for ulcerative lesions of the exterior surface of carapace and plastron elements. Most prior research has described the condition in terms of what organisms were collected from within the lesions. Those studies identified a wide variety of vectors associated with shell disease, including fungi, algae, trematodes, bryozoans, and numerous bacteria (Hunt, 1957; Garner et al., 1997; Hutchinson and Frye, 2001; Jacobson, 2007; Rothschild et al., 2013). However, concerns arise regarding whether these organisms are the proximate cause of the lesions or if they were introduced after the scutes had been compromised and allowed other organisms access to the underlying bone. In at least some cases, ectoparasites such as leeches could initiate the sequence of succession among vectors, culminating in these suites of pathologies (Zonneveld and Bartels, 2022).

Shell disease has been identified in the fossil record, but many of those identifications are tentative and anecdotal (Hutchinson and Frye, 2001; Scheyer, 2009; Cerda et al., 2016). Bite marks, however, on fossil turtle shell are far more widely documented in the literature (e.g., Fuentes, 2003; Karl and Tichy, 2004; Mead et al., 2006; Steadman et al., 2007; Milàn et al., 2011; Evgen et al., 2012; Noto et al., 2012; Morgan and Albury, 2013; Botfalvai et al., 2014, 2015; Hastings et al., 2015; deValais et al., 2020), but many of those represent punctures and furrows, deeply penetrative marks that are often associated with obvious fracturing (sensu Binford, 1981). The shallower pits and scores that have less extreme compression and cracking associated with them pose more of a concern regarding convergence with shell disease (e.g., Hutchinson and Frye, 2001; Chamberlain and Corsini, 2006-2007; Rothschild et al., 2013; Zonneveld and Bartels, 2022). This is compounded by the fact that even the descriptive terms used to describe both types of bone modifications, mainly pits and scores (sensu Binford, 1981), overlap.

Here we present known examples of both bite marks and shell disease on modern examples of the pond slider, *Trachemys scripta*, and fossil examples of turtle shell fragments from the Cenomanian of north-central Texas with putative bite marks and shell disease (Noto et al., 2012; Adams et al., 2017; Adrian et al., 2019). We characterize and compare the surficial expression of these modifications as well as internal textures using microcomputed tomographic (μCT) imaging in order to differentiate and diagnose these two convergent processes.

Institutional Abbreviations: DMNH, Perot Museum of Nature and Science, Dallas, Texas, USA. SAAF, St. Augustine Alligator Farm and Zoological Park, St. Augustine, Florida, USA. UTK, University of Tennessee Department of Anthropology Vertebrate

Skeletal Comparative Collection, Knoxville, Tennessee, USA.

MATERIALS AND METHODS

Identification of Bite Marks

Vertebrate bite marks on bone represent impact damage formed when a tooth interacts with the target surface, resulting in deformation. The extent of this modification is governed by the size and shape of the impacting tooth, the force of impact, and the strength of the impacted surface, which is largely controlled by the relative thickness of the dense cortical bone (Drumheller and Brochu, 2016). Across toothed vertebrates, these traces are characterized by being stereotypically U- or V-shaped in cross section and by exhibiting some degree of crushing, compaction, and fracturing associated with the impacting event (Binford, 1981). The specific morphology of each mark is governed by the shape of the impacting tooth, its depth of penetration, and its movement relative to the surface of the bone. An impact with no lateral movement will result in a mark that broadly reflects the shape of the tip of the tooth. These traces are broadly divided into shallow pits, which do not fully penetrate the cortical bone, and deeper punctures, which fully pierce through the cortical bone into the trabecular bone beneath. Lateral movement of the tooth along the surface of the bone will result in an elongate mark, again subcategorized by whether it only indents the cortical bone (=scores) or pierces it fully (=furrows) (Binford, 1981).

This generalized bite mark classification scheme centered on these four basic bite mark types – pits, punctures, scores, and furrows – can be expanded to include descriptions of the specific morphologies of each, as governed by the trace maker's dental morphology and associated biting behavior. For example, the serrated teeth of ziphodont groups often leave striated marks, parallel impressions of the individual impacting denticles (e.g., Fiorillo, 1991; Rogers et al., 2003; D'Amore and Blumenschine, 2009; Hone and Rauhut, 2010; Paik et al., 2011; Farlow and Holtz, 2012; Noto et al., 2012), whereas mammalian molars can leave complex marks reflecting the shapes and spacing of the cusps of individual teeth (e.g., Haynes, 1983; Domínguez-Solera and Domínguez-Rodrigo, 2009; Saneyoshi et al., 2011). This classification scheme is rooted in prior taphonomic work, and therefore uses the non-genetic definition of 'mark,' meaning that this term does not denote a biotic or abiotic source in the absence of a modifying term, such as 'bite' (sensu Zonneveld et al., 2022).

All of the bite marks sampled in our analysis are associated with crocodyliform actors: *Mecistops cataphractus* in the modern sample (Figure 1) and *Deltasuchus motherali* in the fossil specimens (Figures 2 and 3; Noto et al., 2012; Adams et al., 2017; Drumheller et al., 2021). These species both exhibit plesiomorphic crocodylian dentition in the form of conical, strongly carinated teeth. This morphology is reflected in bite marks as roughly circular to oval indentations, of which roughly 10% exhibit a subscore or bisection caused by the carina in relatively freshly erupted teeth. These bisected marks are considered diagnostic of bite marks generated by crocodylians (Njau and Blumenschine, 2006; Drumheller and Brochu, 2014; 2016; Njau and Gilbert, 2016) and are present in the modern specimen sampled here. The presence of similar marks, partnered with the more general crushing, as well as interdental spacing consistent with the dentition of *Deltasuchus*, served as the original justification for associating the traces on fossil specimens DMNH 2013-07-1319 and DMNH 2013-07-0563 with that crocodyliform actor (Noto et al., 2012; Adams et al, 2017; Drumheller et al., 2021).

The gross morphology of each individual tooth mark may be further modified by associated fracturing. None of the fossil specimens observed here exhibit extensive fracturing beyond crushing within the immediate margins of each mark. However, the modern specimen (SAAF) has a large, radiating fracture that connects a series of punctures along the shell's carapace; this arcing line of tooth marks is interpreted as a serial bite mark, i.e., a set of tooth marks generated together during a single biting event (Figure 1). Radiating and depressed fractures, in which the bone surrounding the point of impact collapses under the force of the bite, are commonly associated with bites that are powerful enough to compromise the structural integrity of the bitten surface (Njau and Blumenschine, 2006; Drumheller and Brochu, 2014).

The internal expression of the modern and fossil bite marks examined here should all reflect crushing, impact, and displacement of the dense, outermost layer of cortical bone deeper into the body of the bite mark. Such damage is predicted to be visible in the unaltered µCT data and especially in the Look-Up Table (LUT) heatmap representations of internal variation in sample density, even in the shallower pits and scores, which are thought to be most convergent with shell disease. Details of

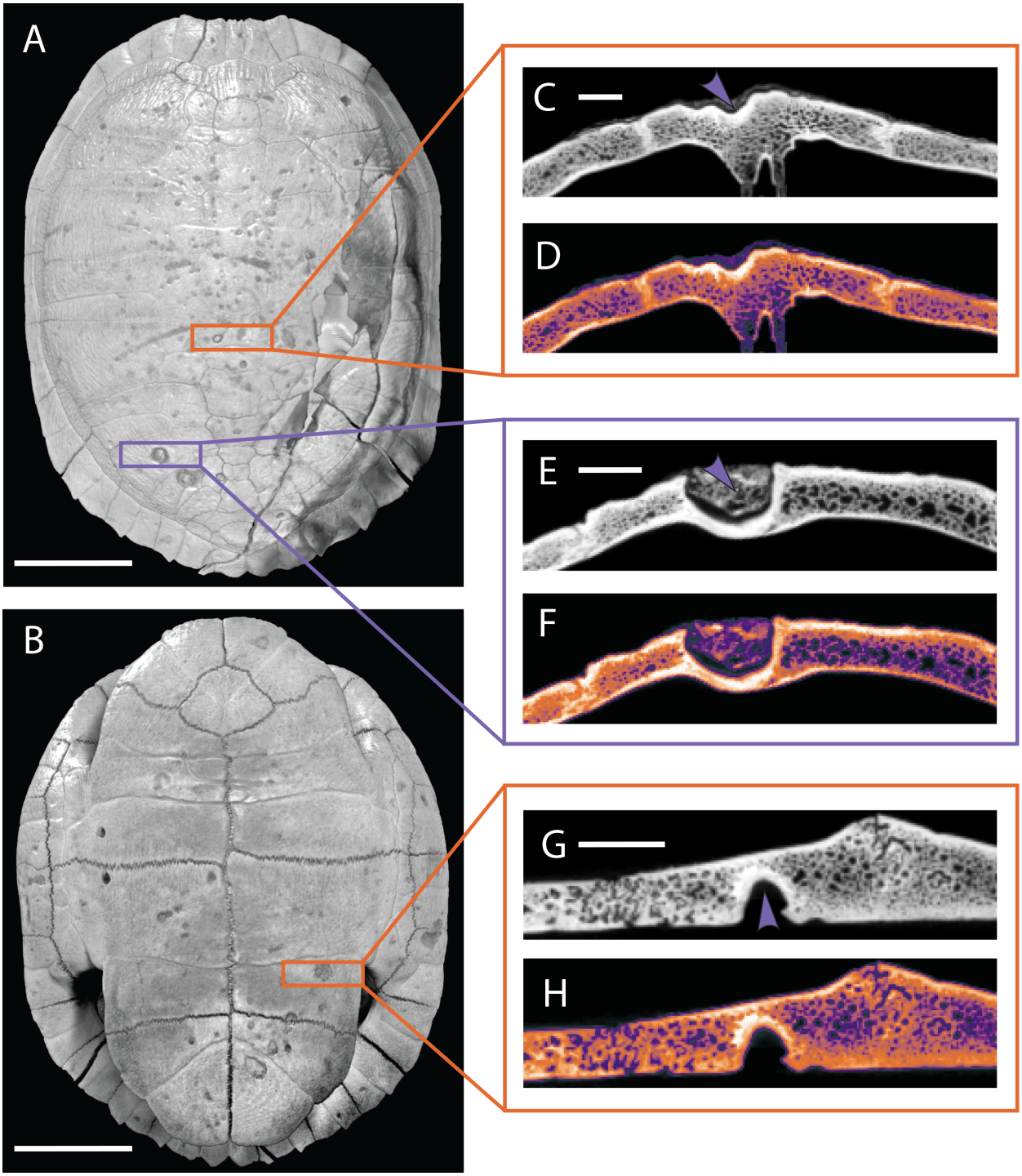

FIGURE 1. Modern *Trachemys scripta* shell (SAAF) with bite marks attributed to *Mecistops cataphractus.* Orthographic models of the shell, based on µCT data shown in dorsal (A) and ventral (B) views. Frames on the models highlight specific bite marks, shown on the right as both direct µCT data (C, E, G) and heatmapped slices illustrating bone density changes (D, F, H). In the heatmapped cross sections, colors range from purple (lowest density), to orange (medium density), to white (highest density). Specific bite marks are indicated with purple arrows. Scale bars in A and B equal 5 cm. Scale bars in C, E, and G equal 5 mm.

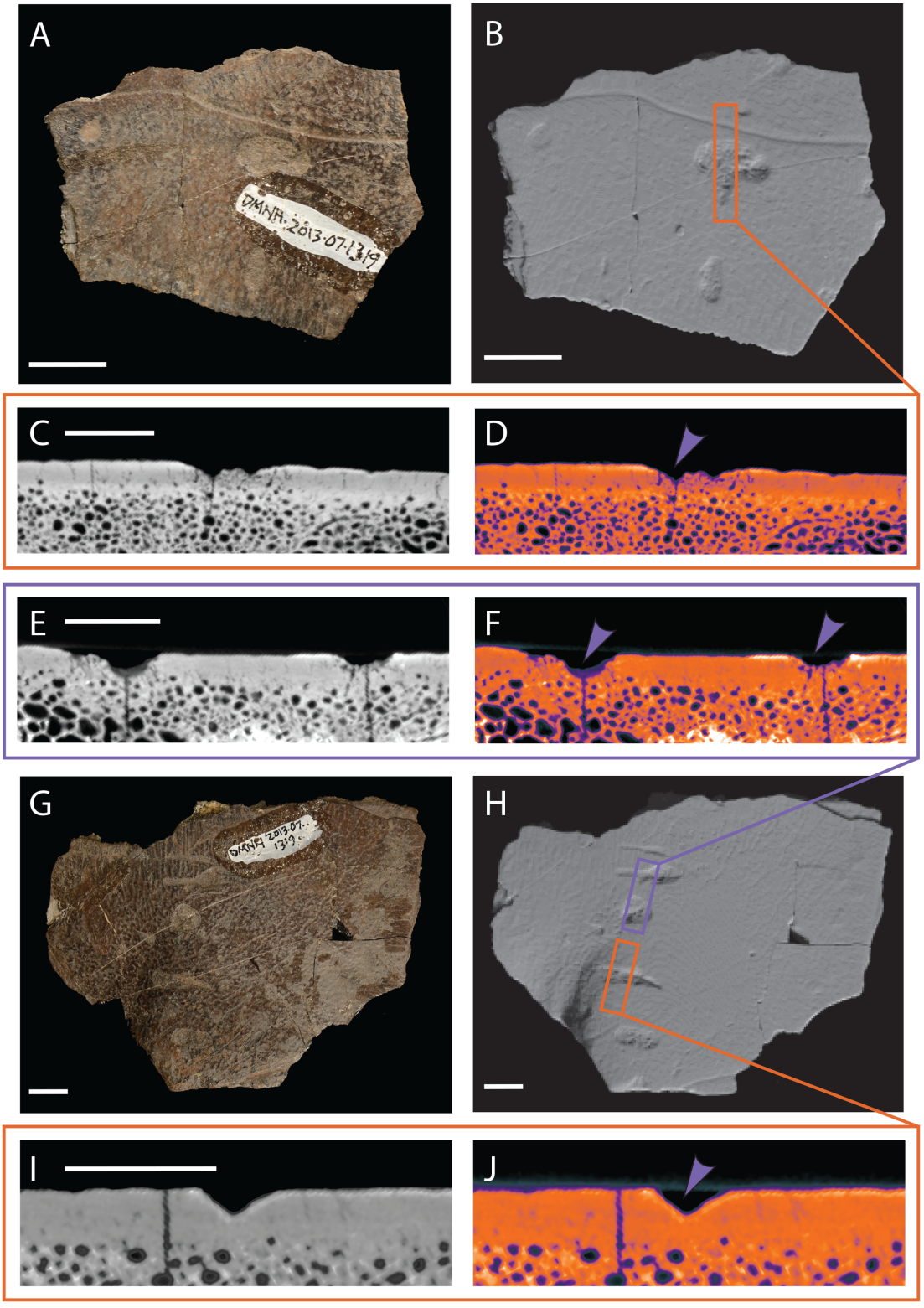

FIGURE 2. Fossil turtle shell fragments (DMNH 2013-07-1319) with putative bite marks. Photographs (A, G) and orthographic models based on µCT data (B, H) shown in external view. Frames on the photograph and model highlight specific areas with bite marks as both direct µCT data (C, E, I) and heatmapped slices illustrating bone density changes (D, F, J). In the heatmapped cross sections, colors range from purple (lowest density), to orange (medium density), to white (highest density). Specific bite marks are indicated with purple arrows. Scale bars in A, B, G, and H equal 2 cm. Scale bars in C, E, and I equal 5 mm.

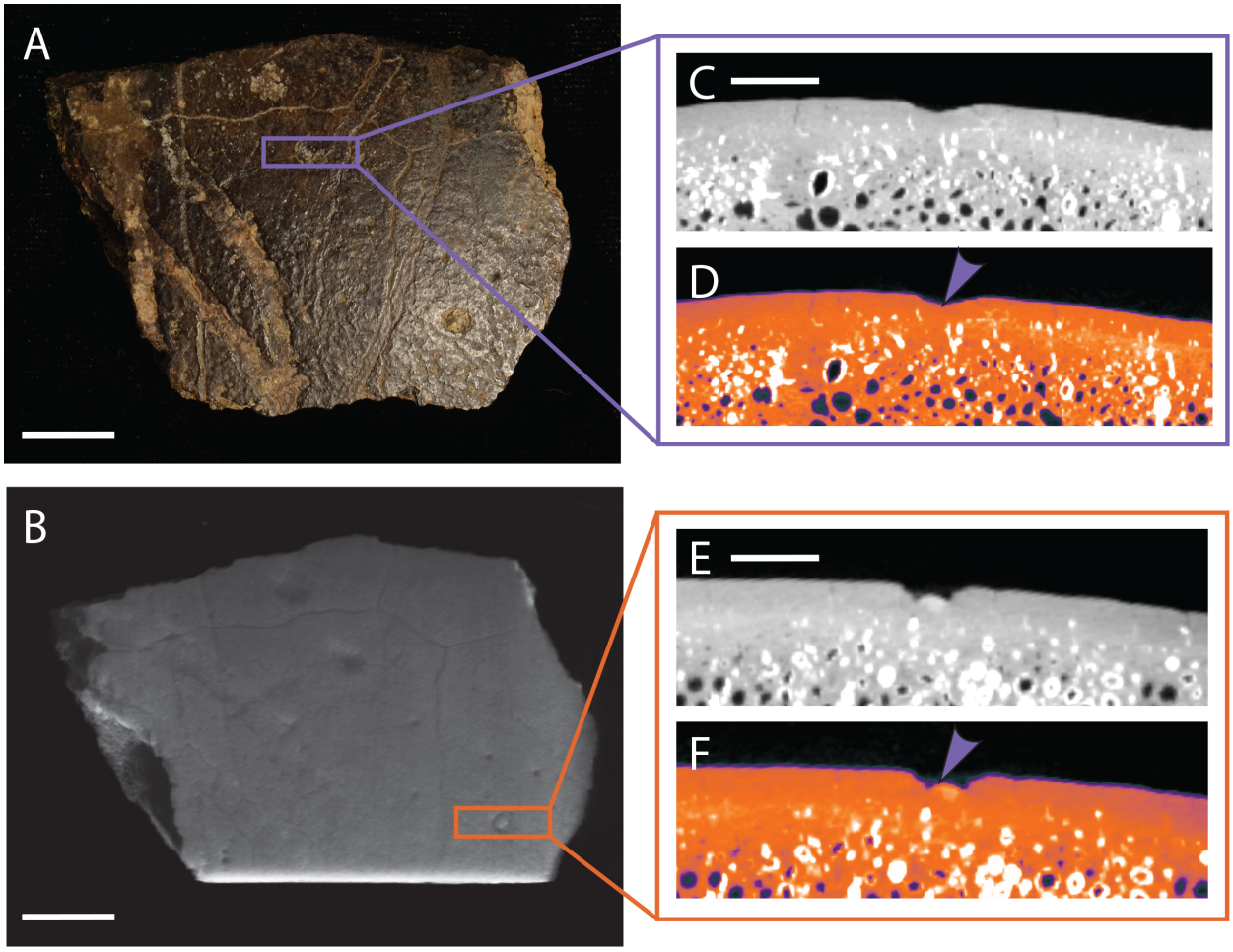

FIGURE 3. Fossil turtle shell fragment (DMNH 2013-07-0567) with putative bite marks. Photograph (A) and orthographic model based on µCT data (B) shown in external view. Frames on the photograph and model highlight specific areas with bite marks as both direct µCT data (C, E) and heatmapped slices illustrating bone density changes (D, F). In the heatmapped cross sections, colors range from purple (lowest density), to orange (medium density), to white (highest density). Specific bite marks are indicated with purple arrows. Scale bars in A and B equal 2 cm. Scale bars in C and E equal 5 mm.

this visualization method are described in detail below.

Identification of Shell Disease

Though basic descriptions of the morphology associated with modern shell disease remain rare, a recent description of pathologies in modern *Trachemys scripta* carapace and plastron elements provides a basis of comparison for positively identifying this poorly understood suite of pathologies (Zonneveld and Bartels, 2022). Even though the proximate cause of many examples of shell disease is still poorly understood, the pathology itself occurs in a predictable, generalized pattern, no matter the inciting event or infection.

Shell disease is most commonly expressed as small (1-5 mm), hemispherical depressions that do not fully penetrate the cortical bone. The external margins of these less advanced lesions are usually smooth and rounded or flat-bottomed (Zonneveld and Bartels, 2022), but some can exhibit a raised margin or lip around their perimeter. In more extreme cases, shell disease can etch further into the overlying layer of cortical bone, exposing the spongey trabecular bone beneath it. In advanced deterioration of the bone, the interior surface of the pathology can take on an even more irregular, bubbly appearance. These pathologies are usually round in outline, though neighboring lesions can merge into larger affected patches. More irregular associations of these pathologies have been called pit clusters, whereas other times the associations take on a more regular association, organizing into

shallow, circular structures called ring traces (Zonneveld and Bartels, 2022).

Known examples of this type of advanced shell disease are present on both of our modern specimens, UTK 2317 and UTK 1844 (Figures 4 and 5). The internal expressions of these more extreme examples are not particularly convergent with bite marks, even in hand sample under little to no magnification. The less advanced examples of shell disease are more convergent with bite mark damage. Shallow, rounded lesions that do not penetrate the cortical bone are superficially similar to non-penetrative bite marks, and historically both have been called pits and scores (e.g., Hunt, 1957; Lovich et al., 1996; Garner et al., 1997; Jacobson, 2007; Zonneveld and Bartels, 2022). The margins of these lesions can be flush with the surrounding unaffected bone, and if there is a raised lip, it is subtle. The interior surfaces of these lesions can be quite smooth, sometimes making differentiation from the compressed interiors of shallow bite marks challenging, even under magnification. This type of expression is apparent on the fossil specimen DMNH 2013-07-0563, which led to its tentative interpretation as shell disease (Figure 6).

Again, we predict that this type of etching damage should be visually diagnosable from bite marks, based on the absence of associated compression related to the crushing or impact damage characteristic of bite marks in both unaltered µCT data and especially in the LUT heatmap representations, described in detail below.

Modern Specimens

Modern turtle shells with known examples of shell disease and bite marks were observed in order to provide a baseline upon which to compare these two types of bone modifications. A large pond slider (*Trachemys scripta*) died as the direct result of an incidental attack by an African slender-snouted crocodile (*Mecistops cataphractus*) at the Saint Augustine Alligator Farm and Zoological Park (SAAF), St. Augustine, Florida, USA. (Figure 1). Its skeletal material preserves bite marks on the carapace and plastron; multiple pits and punctures (sensu Binford, 1981) are present, some of which display bisections, which are diagnostic of crocodyliform bite traces (e.g., Njau and Blumenschine, 2006; Drumheller and Brochu, 2014; 2016; Njau and Gilbert, 2016). The carapace of this specimen also has a partial fracture in the most highly bite marked region of the shell, which was associated with the high forces generated during crocodylian bites (Erickson et al., 2012; 2014; Gignac and Erickson, 2016).

In order to facilitate comparison between modern specimens and to remove any clade-specific variables from our modern dataset, we also selected additional specimens of *Trachemys* with known examples of shell disease (UTK 2317 and UTK 1844) for inclusion in our study. The prevalence of shell disease is well documented in this species (Garner et al., 1997), the only previous detailed morphological description of shell disease was based on specimens of this taxon (Zonneveld and Bartels, 2022), and both specimens exhibit extensive remodeling consistent with typical examples of shell disease. These specimens are partially disarticulated; all shell elements were observed under low magnification, but only portions of the shells were selected for further exploration using CT scanning. Those selected were mainly the plastron from UTK 2317 (Figure 4) and the articulated plastron and partial carapace from UTK 1844 (Figure 5).

Fossil Specimens

The fossil specimens described here (DMNH 2013-07-1319, DMNH 2013-07-0567, DMNH 2013-07-0563) were all collected from the Arlington Archosaur Site (AAS), a fossil-rich locality in north Texas, situated within the Dallas-Fort Worth metroplex (Figure 7). The AAS sits within the Lewisville Formation of the upper Woodbine Group, placing it in the early middle Cenomanian (~96 Ma) (Kennedy and Cobban, 1990; Emerson et al., 1994; Gradstein et al., 2004; Ambrose et al., 2009; Donovan et al., 2015). The main, fossil-bearing horizon (Facies A *sensu* Adams et al., 2017) preserves a rich deltaic ecosystem with estuarine and coastal influences. The mixed terrestrial, freshwater, and saltwater input at the site is reflected in a taxonomically diverse assemblage, which includes numerous plant macro- and microfossils, molluscs, crustaceans, elasmobranchs, lungfish and other bony fishes, lissamphibians, mammals, and dinosaurs (Noto et al., 2012; Adams et al., 2017; Noto et al., 2020; Drumheller et al., 2021). Most relevant to our study, the AAS is particularly rich in turtles, belonging to at least four taxa (Adrian et al., 2019), crocodyliforms from at least four separate clades (Adams et al., 2017; Noto et al., 2020; Drumheller et al., 2021), and numerous feeding traces (Noto et al., 2012).

The turtle assemblage includes specimens attributable to the following clades: Trionychidae, *Algorachelus*, *“Trinitichelys” maini*, and *Naomiche-*

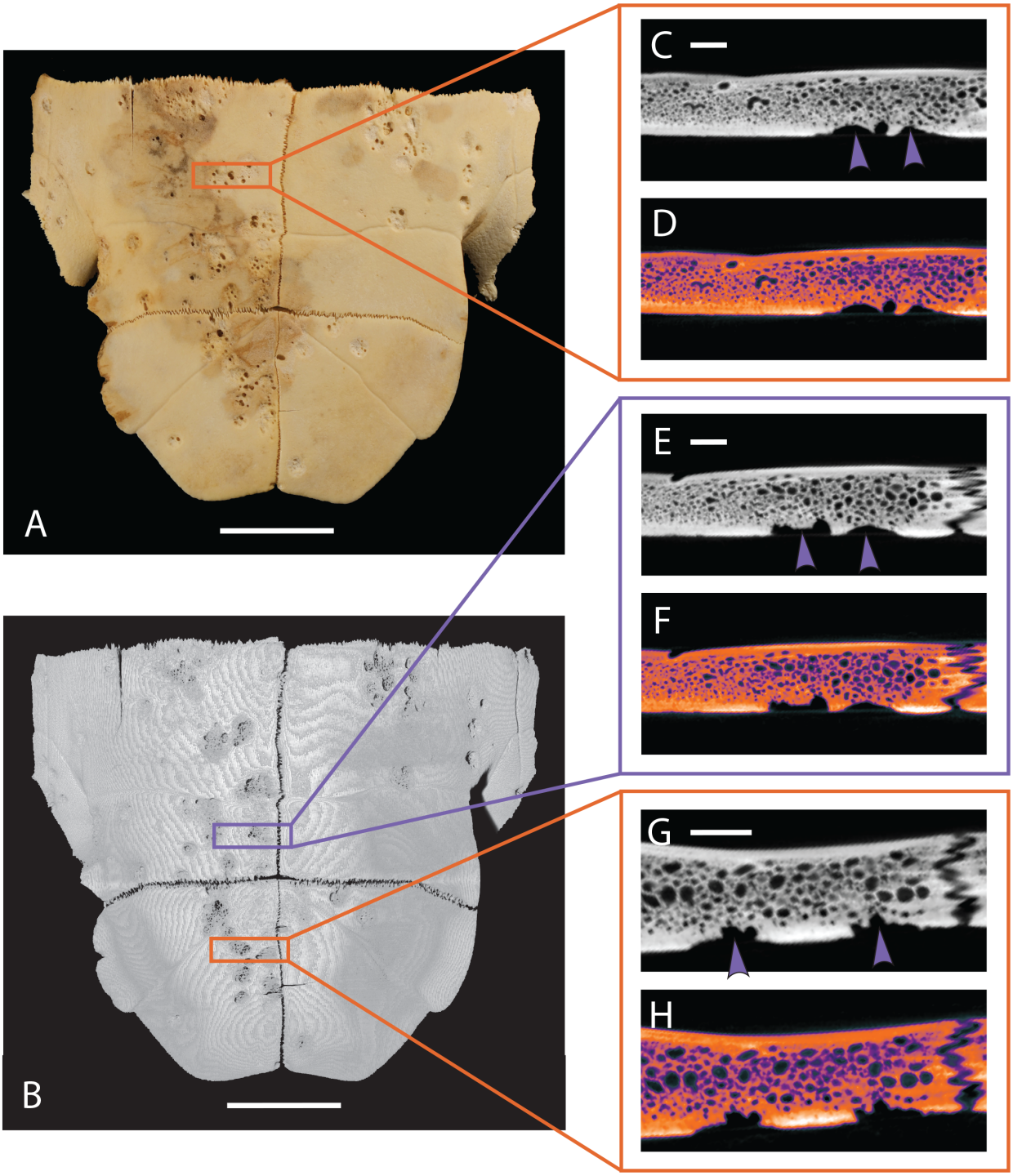

FIGURE 4. Modern *Trachemys scripta* plastron elements (UTK 2317) with shell disease. Photograph (A) and orthographic model based on µCT data (B) shown in ventral view. Frames on the photograph and model highlight specific areas of shell disease, shown on the right as both direct µCT data (C, E, G) and heatmapped slices illustrating bone density changes (D, F, H). In the heatmapped cross sections, colors range from purple (lowest density), to orange (medium density), to white (highest density). Patches of shell disease are indicated with purple arrows. Scale bars in A and B equal 5 cm. Scale bars in C, E, and G equal 5 mm.

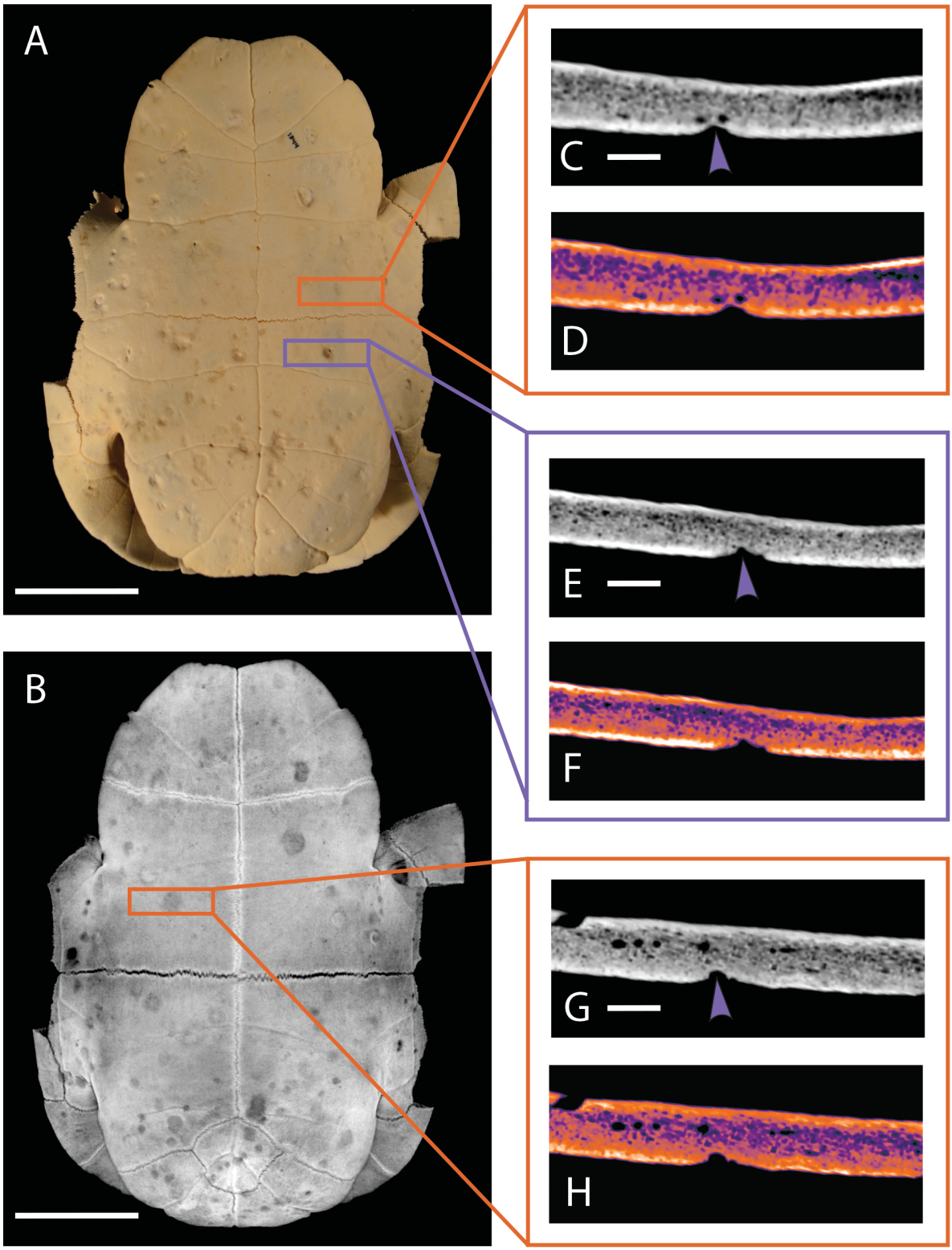

FIGURE 5. Modern *Trachemys scripta* plastron and partial carapace elements (UTK 1844) with shell disease. Photograph (A) and orthographic model based on µCT data (B) shown in ventral view. Frames on the photograph and model highlight specific areas of shell disease, shown on the right as both direct µCT data (C, E, G) and heatmapped slices illustrating bone density changes (D, F, H). In the heatmapped cross sections, colors range from purple (lowest density), to orange (medium density), to white (highest density). Patches of shell disease are indicated with purple arrows. Scale bars in A and B equal 5 cm. Scale bars in C, E, and G equal 5 mm.

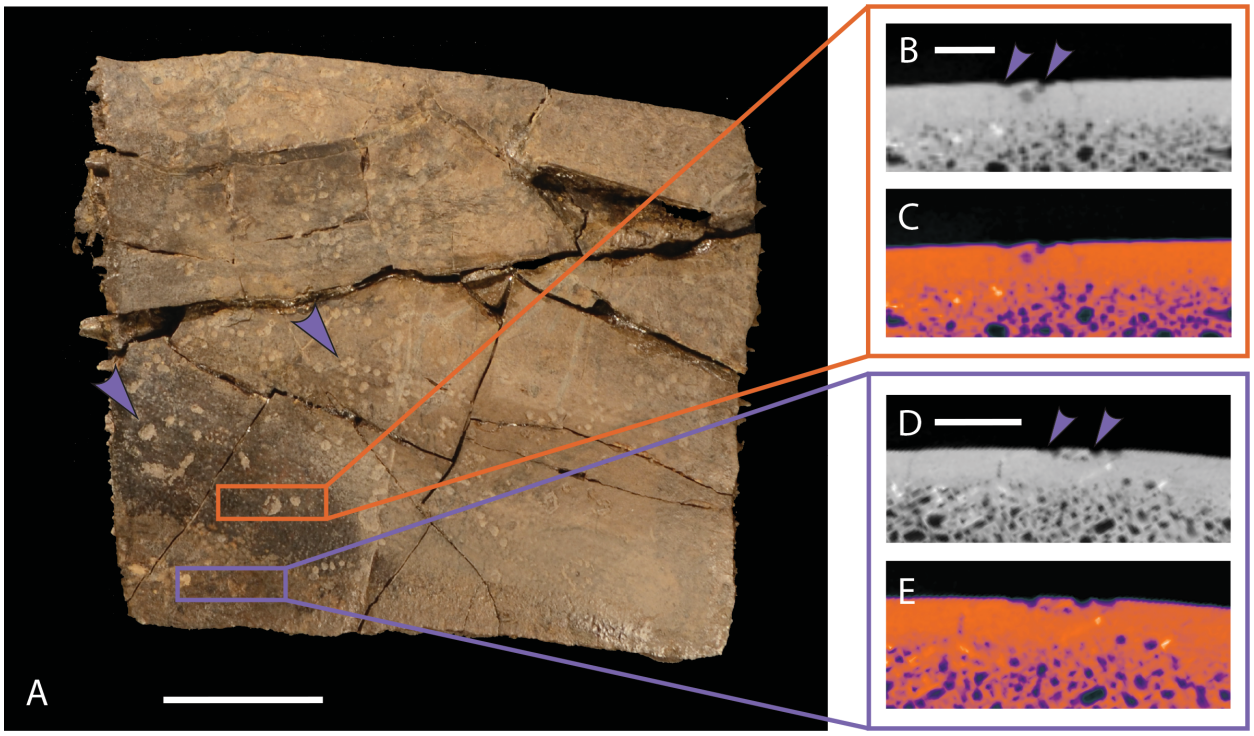

FIGURE 6. Fossil turtle shell fragment (DMNH 2013-07-0563) with putative shell disease.. Photograph (A) shown in external view. Frames on the photograph and highlight specific areas with shell disease as both direct µCT data (B, D) and heatmapped slices illustrating bone density changes (C, E). In the heatmapped cross sections, colors range from purple (lowest density), to orange (medium density), to white (highest density). Specific patches of shell disease are indicated with purple arrows. Scale bar in A equals 2 cm. Scale bars in B and D equal 5 mm.

lys (Adrian et al., 2019). Several shell specimens exhibit pathologies, and a subset of injuries associated with apparent impact trauma (Figures 2 and 3) previously were identified as bite marks attributable to the neosuchian crocodyliform *Deltasuchus motherali* (Noto et al., 2012; Adams et al., 2017; Drumheller et al., 2021). These marks were identified based on the presence of crushing, impact damage within the pits, punctures, and scores identified on the shells (sensu Binford, 1981), and further associated with the crocodyliform actor based on the presence of bisected marks (sensu Njau and Blumenschine, 2006; Drumheller and Brochu, 2014; 2016; Njau and Gilbert, 2016) and a comparison of the spacing of identified serial marks to the interdental spacing of *Deltasuchus* specimens (Noto et al., 2012).

However, some of the rounded or elongate depressions on other shells initially observed in the assemblage notably lacked the traces of crushing and impact damage that characterize bite marks (sensu Binford, 1981). Rather, the smooth, somewhat raised lips of some of these features, their irregular internal surface structure, and their pattern of expression (largely random distributions punctuated with a small number of tightly spaced, linear or circular arrangements) supported their preliminary identification as shell disease, which we seek to test in this study (Figure 6).

It is important to note that in the time since the initial description of these specimens (Noto et al., 2012) and the current study, the fossils were moved from the University of Texas at Arlington to the Perot Museum of Nature and Science, resulting in a change of specimen identification numbers. To better facilitate comparisons between previous publications and the current study, taxonomic identifications along with both previous and current specimen identification numbers for each modified fossil have been gathered into Table 1.

Computed Tomographic Imaging

Computed tomographic (CT) scanning previously has shown promise in interpreting more diagnostic types of bone surface modifications (e.g., Boyd et al., 2013; Drumheller et al., 2014; de Valais et al., 2020). Given the disparate processes, which lead to the formation of bite marks and shell disease, it is likely that internal visualization and comparisons of modern, known examples of these

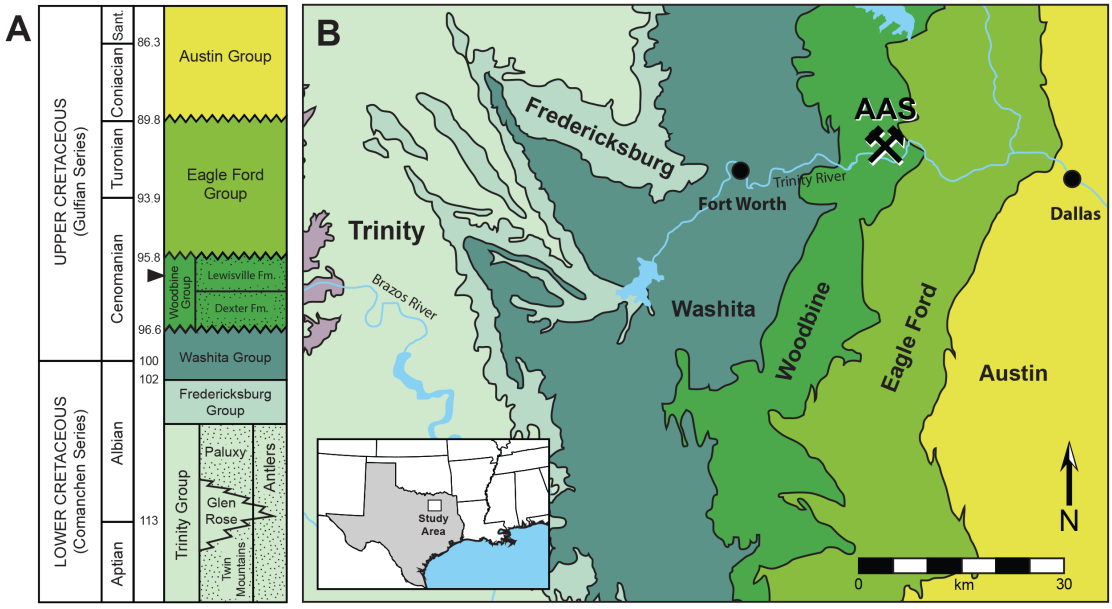

FIGURE 7. Location and geologic position of the Woodbine Group. A. General stratigraphic sequence and timescale for the Cretaceous of central and north central Texas showing the position of the Woodbine Group. Position of the AAS within the Woodbine is marked with an arrowhead. Terrestrial deposits represented by stippled intervals. Time scale based on Denne et al. (2016). Modified from Adams et al. (2011). B. Generalized map of geological units present as surface exposures in the Fort Worth basin with location of AAS shown. Modified after Strganac (2015) and Barnes et al. (1972).

damage types with putative fossil exemplars might prove illuminating. Therefore, both modern and fossil examples of shell disease (UTK 2317, UTK 1844, and DMNH 2013-07-0563) and bite marks (SAAF *Trachemys*, DMNH 2013-07-0567 and DMNH 2013-07-1319) were selected for further analysis. Each specimen was µCT scanned with a Nikon XTH 225 ST scanner at the Shared Materials Instrumentation Facility (SMIF) at Duke University, and X-ray radiographs were reconstructed as .TIFF files using Nikon CT Pro 3D software. Scanning parameters are listed for each specimen in Table 2. All digital data and associated models for this study are available at Morphosource.org (Project 503210).

Visualization of the interior textures of affected regions of each shell was performed with the Dragonfly image processing software. Bone textures were further interpreted using the program's LUT function that assigns colors based on scalar values of the imaged material, in this case bone density. This process creates a density heatmap, visually emphasizing differences in the internal structure of each sample either due to natural zones of variation, as in the transition from cortical to trabecular bone, or to pathological alteration of the underlying tissues, as in both bite marks (Figures 1, 2, and 3) and shell disease (Figures 4, 5, and 6). Measurements of unaffected vs. affected cortical bone thicknesses, maximum depth of mark penetration, and maximum width of affected bone surface were made using the image processing software ImageJ (Schneider et al., 2012). These results are reported in µm in Table 3.

RESULTS

SAAF *Trachemys scripta*

The modern bite marked specimen (Figure 1: SAAF *Trachemys*) is 24.5 cm long and 19 cm wide. Some of the keratinous scutes are still in place, especially on the carapace, which obscures some of the underlying individual tooth marks in the bone (Figure 1A). A line of serial bite marks is associated with a radiating fracture that extends from midline on the posterior margin of the carapace anteriorly roughly two-thirds the length of the shell, angling to the right and terminating roughly halfway between the shell's midline and its right lateral margin. Smaller, associated fractures radiate from this main break, one propagating posterolaterally towards the right margin of the shell and others forming a concentric, depressed region along the right margin of the longest fracture. A 44.61 mm by 15.19 mm D-shaped fragment of the carapace was displaced and lost some time prior to collection.

TABLE 1. Previous field numbers, current specimen identification numbers, element and taxonomic identification of each element. * = taxonomic revisions based on Adrian et al., 2019.

Field Number (Noto et al., 2012)	DMNH Specimen Number	Element	Taxonomic Notes
UTA-AASO-125	2013-07-0358	Femur	*Protohadros byrdi*
UTA-AASO-201	2013-07-0521	Femur	*Naomichelys* sp.*; previously identified as ornithopod
UTA-AASTL-001	2013-07-0783	Right bridge	*"Trinitichelys" maini**
UTA-AASTL-002	2013-07-0704	Right bridge	*"Trinitichelys" maini**
UTA-AASTL-003	2013-07-0696	Right bridge	*"Trinitichelys" maini**
UTA-AASTL-008	2013-07-0560	Anterior peripherals	*"Trinitichelys" maini**
UTA-AASTL-012	2013-07-0710	Bridge	*"Trinitichelys" maini**
UTA-AASTL-013	2013-07-0690	Xiphiplastron	*"Trinitichelys" maini**
UTA-AASTL-014	2013-07-0675	Carapace	*"Trinitichelys" maini**
UTA-AASTL-015	2013-07-0687	Carapace	cf. *"Trinitichelys"**
UTA-AASTL-016	2013-07-0685	Shell fragment	cf. "*Trinitichelys"**
UTA-AASTL-020	2013-07-0686	Costal	*Naomichelys* sp.*
UTA-AASTL-025	2013-07-0568	Carapace	*"Trinitichelys" maini**
no number (associated with 012)	2013-07-0710	Shell fragment	*"Trinitichelys" maini**
UTA-AASTL-007	2013-07-0711	Hyoplastron	*Naomichelys sp.**
UTA-AASTL-009	2013-07-0561	Carapace	
UTA-AASTL-005	2013-07-0558	Posterior peripheral	*Naomichelys* sp.*
UTA-AASTL-006	2013-07-0559	Left costal 7	*Naomichelys* sp.*
UTA-AASTL-024	2013-07-0567	Shell fragment	*Naomichelys* sp.*

TABLE 2. µCT scanning parameters for specimens included in this study.

Specimen	kV	µA	Filter	Exposure Time	Voxel size
DMNH 2013-07-0563	205	322	0.75 copper	267 ms	0.06622 mm
DMNH 2013-07-0567	210	288	0.75 copper	267 ms	0.06126 mm
DMNH 2013-07-1319	210	278	0.75 copper	267 ms	0.05895 mm
UTK 2317	150	567	0.25 copper	267 ms	0.09242 mm
UTK 1844	145	684	0.25 copper	267 ms	0.09980 mm
SAAF unnumbered	150	688	0.25 copper	267 ms	0.10399 mm

Four individual tooth marks (widths of 3.59 mm, 4.87 mm, 5.03 mm, 6.11 mm) are visible along the margin of this break, but the fracture, the ventral displacement of the right margin along that break, and the missing fragment of bone make reliable measurements of each tooth mark problematic. A single, bisected puncture (7.41 mm long by 4.70 mm wide) is present roughly 3.5 cm from the shell's right margin and 4.5 cm posterior to the anteriormost edge. This rounded, slightly fusiform puncture is approximately aligned with the others, 5 cm anterior to the termination of the break.

On the plastron, four additional punctures occur 2 cm medial to the right bridge (Figure 1B). The anteriormost and posteriormost of these serial marks are shallow pits, and the two centrally situated marks are deeper bisected punctures, measuring from anterior to posterior 4.33 mmby 3.07 mm and 4.63 mm by 3.16 mm (Figure 8A). The spacing between these four marks, again progressing anterior to posterior and measured from the center of each depression, are: 17.53 mm, 19.18 mm, and 18.70 mm. The positions of these serial marks suggest they were formed concurrently with the serial marks on the carapace

TABLE 3. Measurements of unmodified and modified shell regions. Cortical bone thickness = average of unmodified region of bone immediately to the left and right of the modified region, taken from µCT slices representing the region of maximum mark penetration into the cortical bone. Pathology thickness = thickness of the observed cortical bone at the point of maximum mark penetration. Note, measurements of 0 are recorded when trabecular bone is exposed in the bottom of the mark, measurements of 0* represent specimens in which the affected bone has fractured, leaving a gap in the bottom of the mark. Maximum depth = measured relative to the projected curvature of the surface of the shell, as suggested by the unmodified bone to the immediate to the left and right of the modified region, taken from CT slices representing the region of maximum mark penetration into the cortical bone. Maximum width = the widest diameter of the modified shell region.

Specimen Number	Cortical Bone Thickness (µm)	Pathology Thickness (µm)	Maximum Depth (µm)	Maximum Width (µm)
SAAF	45288.06	56951.04	172647.04	243635.08
	29130.635	62399.93	111264.2	382252.95
	32896.835	54984.73	268506.27	391349.41
	51405.835	0*	0*	178124.16
UTK 1844	24245.115	0	30261.9	109062.13
	25331.58	0	43635.5	157751.88
	25386.99	0	52452.4	184845.27
UTK 2317	45288.21	0	104220.47	431636.55
	41977.59	0	116430.76	339495.79
	42773.075	0	120013.43	283238.1
	42092.27	0	158822.71	377231.37
DMNH 0563	97228.65	0	18505.9	64807.59
	121232.02	0	32351.63	76673.77
	112778.42	0	30624.77	125514.26
DMNH 0567	81907.24	84583.98	84583.98	257895.4
	83234.265	84774.67	36879.82	84774.67
	88745.795	83148.73	28367.22	86037.54
DMNH 1319	139768.74	77083.42	80875.33	201561.55
	107567.655	37105.23	123479.95	463813.03
	120727.92	45855.25	77271.17	468758.1

because they are aligned with one another on opposing sides of the shell. The size and spacing of these serial marks are consistent with the dentition of the crocodylian that had shared the turtle's enclosure: *Mecistops cataphractus*.

An additional bisected pit (2.98 mm by 2.48 mm) is present along the plastron's midline roughly 6 mm to the right of the suture. At least three additional marks, two punctures and one pit, are present near the posterior edge of the plastron. The pit, measuring 3.70 mm by 1.97 mm with no obvious bisection, is located just posterior to the right bridge of the shell and may be associated with the serial bite marks described above. The two punctures are situated on the left side of the plastron. The larger of these is broadly oval shaped with an apparent drag-out mark. Taken together, the total maximum length of that mark is 7.84 mm by 4.32 mm wide. The second puncture is positioned roughly 13 mm lateral to the first and measures 3.90 mm by 3.41 mm with an incomplete bisection in the form of a single notch associated with the impacting tooth's carina on the anterior margin of the long axis of the trace.

There are regions of this plastron that may also preserve shell disease (Figure 1B), one sub-rounded area roughly 29 mm medial to the anteriormost of the serial marks, one 22 mm posterior to the set of two punctures, and a clustering of circular depressions along the right side of the midline, from the center of the plastron towards the posterior margin of the shell. All affected areas are sub-rounded and lack obvious crushing or impact trauma. As such, we tentatively identify these as shell disease, which does commonly affect this taxon (Garner et al., 1997; Zonneveld and Bartels, 2022).

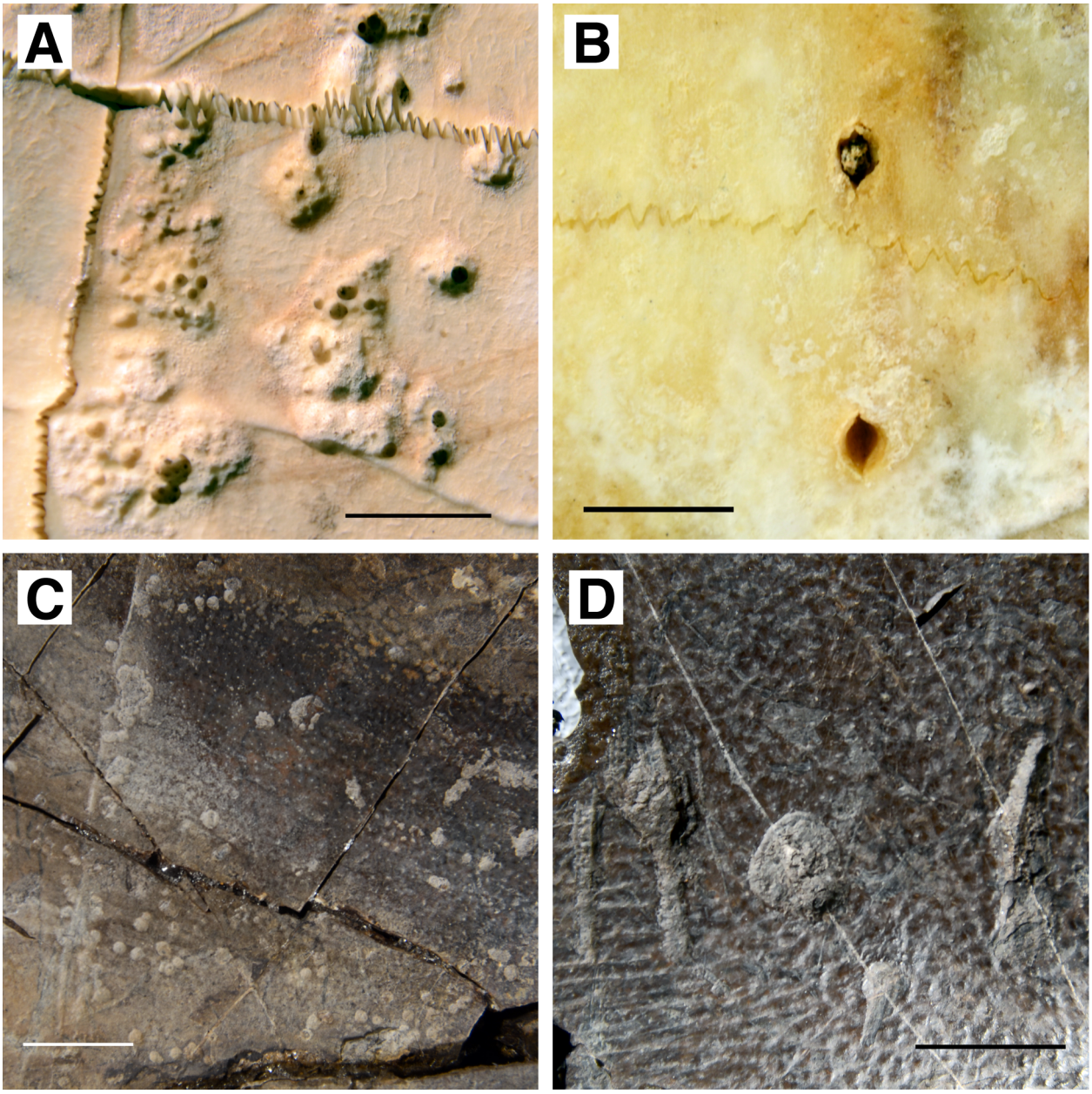

FIGURE 8. Characteristic examples of shell disease and bite marks in modern and fossil turtle shells. Modern shell disease on the plastron of *Trachemys scripta*, specimen UTK 2317 (A). Modern bite marks (bisected punctures) on the plastron of *Trachemys scripta*, specimen SAAF unnumbered (B). Fossil shell disease on a fragment of turtle shell, specimen DMNH 2013-07-0563 (C). Fossil bite marks (four scores and one pit) on a fragment of turtle shell, specimen DMNH 2013-07-1319 (D). Scale bars equal 10 mm.

Internal morphologies show that marks appear V- or U-shaped in cross section, tapering to a rough point. A thick band of compressed cortical bone underlies all punctures (Figure 1C-1H). These bands are visible in plain CT data, and variation in bone density is further highlighted in the LUT heatmap, where compressed regions are consistently expressed as a lighter color than the rest of the surrounding bone tissue (Table 3). Breakage and fracture points also show signs of bone compression, but not to the extent found with individual V-shaped marks. An extreme case in SAAF shows a large, U-shaped puncture located on the carapace exhibiting significant bone compression, enough so that the internal arch of the carapace is bowing inwards. This puncture is surrounded by a thick line of white and bright orange when viewed in LUT heatmap settings.

UTK 1844 and 2317 *Trachemys*

The carapace and plastron of UTK 1844 (Figure 5) are present but largely disarticulated because of the method of skeletonization. The whole plastron and a portion of the anterior rim of the carapace remain in articulation. Because the plastron is the most heavily altered by shell disease, this portion was selected for further CT scanning and observation (Figure 5A and 5B). The pathologies on the plastron of UTK 1844 range from subrounded, pit-like depressions, as small as 1.3 mm in diameter, to more irregularly-shaped, eroded features up to 11.46 mm in width. The modification of the shell is extensive, with well over 100 patches of affected tissue overlapping and adjoining one another, especially in the anterior half of the plastron (Figure 5C-5H). Though the positioning of most of the depressions is largely random, a small number of sets show unusual patterning. One set, 32 mm anterior to the bridge, includes three roughly equally sized (~1.7 mm in diameter) circular depressions arranged equidistantly in a circle. Other patches, especially near the posterior edge of the plastron, are arranged in linear fashion, the margins of one running indistinctly into the next, creating a chain of sub-rounded depressions that form an elongate, score-like feature. These clusters are common in turtles affected by shell disease (e.g., Hunt, 1957; Lovich et al., 1996; Garner et al., 1997; Jacobson, 2007).

The shell of UTK 2317 (Figure 4) was also disarticulated during cleaning and preparation of the bone. The plastron remains in two parts, anterior and posterior halves, which were rearticulated for purposes of photography and CT scanning. The individual patches of shell disease on UTK 2317 are concentrated around the middle and right posterior portions of the plastron (Figure 4A and 4B). Though less numerous than those seen in UTK 1844, many of the affected regions of UTK 2317 are more deeply modified, with the underlying trabecular bone exposed and readily visible at the surface (Figure 8B). It is not known if this difference of expression represents a different source or duration of the shell disease's progression. The smallest depressed regions are roughly 2 mm in diameter, whereas the largest can range up to 19.64 mm long. Again, the affected regions often merge one into the next, making exact counts of distinct patches difficult to quantify.

Internal morphologies of shell disease manifest as bubble-like hollows and pits that appear to etch their way into the underlying bone tissue (Figure 4C-4H). Bubble-like pits are irregular in shape and placement, sometimes occurring on top of one another, and do not show any tapering. Some pits appear to propagate straight down into the bone tissue, whereas others appear wide towards the bone tissue and narrower towards the shell surface. In one example from UTK 1844, the bubble-like hollows appeared within the bone tissue, appearing unconnected to the surface or another closely associated pit. When viewed as a LUT heatmap, the bubble-like pits appear to cut across the dense, outermost layer of cortical bone, suggesting that the modification process did not involve compression (Table 3). Not all pathologies are as diagnostic though; UTK 1844 exhibits ambiguity in a few areas of interest, such as an occurrence of a shallow pit with an outline of bright orange around the indentation typical of the bite mark specimen.

DMNH 2013-07-1319 and DMNH 2013-07-0567: Bite Marks

DMNH 2013-07-0567 (Figure 3) and DMNH 2013-07-1319 (Figure 2) both include two separate fragments of turtle shell. All four were surface collected, so association is based solely on proximity, and there is no reason to assume that the fragments must come from the same individuals. In fact, one of the specimens under DMNH 2013-07-0567 is visually so different from the other, in terms of color, exposure time, and fossilization, it is arguable that it is not associated with the other fragment. Because it also lacks obvious modification to the bone surface, either bite marks or shell disease, it is excluded from further consideration here.

The remaining three fragments have a more typical appearance of fossils found at the AAS. All are chocolate brown in color, grading to darker brown or black in patches. The quality of the surface preservation is high, both of the original texturing of the shell, and the indentations previously identified as bite marks (Noto et al., 2012; Adams et al., 2017; Drumheller et al., 2021). The remaining specimen assigned as DMNH 2013-07-0567 is roughly rectangular in outline (Figure 3). It measures 70.26 mm in its longest axis and 50.57 mm perpendicular to that. The shell is roughly 12.40 mm at its thickest point, grading down to 7.50 mm at its thinnest. Surficial sculpturing and curvature suggest this fragment came from the carapace, and a broken region on the interior surface suggests its proximity to the bridge. Previously identified bite marks include three pits, all roughly aligned, suggesting a possible serial bite mark

(Figure 3C-3F), and three scores, which are all truncated by the broken edges of the fragment. The pits were all measured along their longest axis and then perpendicular to that, reported as the following lengths and widths: 4.92 mmby 4.74 mm, 3.95 mm by 3.40 mm, and 5.29 mm by 3.40 mm. The scores are 4.16 mm, 4.21 mm, and 4.75 mm wide at the middle of their best preserved sections, and the lengths are all truncated by fractures, with the longest score being 52.25 mm long. None of these marks are bisected, but all exhibit characteristic crushing damage.

The internal morphology of DMNH 2013-07-0567 exhibits many V-shaped indentations in the bone surface (Figure 3C-3F). These marks appear regular in shape and depth, with no associated irregular pits or hollows within the bone structure. There are faint discernable outlines of bone compression in both the plain CT and LUT heatmapped cross section images (Table 3).

Both fragments of DMNH 2013-07-1319 exhibit broad, flat surfaces consistent with plastron fragments (Figure 2). The larger of the two also exhibits a slightly curved margin consistent with proximity to the hinge (Figure 2G and 2H). It has an irregular, fractured margin, measuring 90.38 mm at its widest point and 68.41 mm perpendicular to that. There are six total bite marks on this specimen, five of which are aligned along the curved portion of the surface. These include four scores and one pit, all aligned in a way that suggests a serial bite (Figure 8D). The scores' maximum lengths vs. widths are as follows: 12.12 mm by 2.01 mm, 16.29 mm by 4.24 mm, 16.67 mm by 4.34 mm with a prominent bisection, and 10.43 mm by 4.60 mm. The pit is sub-rounded and 7.64 mm in diameter. The final score is offset from the others, spaced roughly between the pit and bisected score. It measures 6.23 mm by 2.55 mm.

The smaller fragment is also irregularly shaped with a maximum length of 62.64 mm and a width measured perpendicular to that of 47.76 mm (Figure 2A and 2B). It has two pits and two scores. Two of the marks are slightly obscured by the object ID number, but this does not hinder measuring maximum length and width: 13.63 mm by 7.96 mm and 8.49 mm by 3.82 mm. The remaining two marks include one pit (4.48 mm in diameter) and one score with a prominent drag-out or puncture and pull trace that is truncated by the margin of the fracture (maximum measurable length is 13.02 mm, width is 3.56 mm). None are bisected, but the score has associated microstriations (sensu Njau and Gilbert, 2016; Drumheller et al., in press).

When viewed as CT data, the indentations on both fragments of DMNH 2013-07-1319 are regular and roughly V-shaped (Figure 2C-2F and 2I-2J). Similar to what can be seen in hand, in CT scans these V-shaped indentations are aligned along the surface of the larger fragment, regularly spaced and similar in puncture depth. There are faintly discernable outlines of bone compression visible for both fragments in plain CT and LUT heatmapped data (Table 3).

DMNH 2013-07-0563: Shell Disease

This carapace fragment of DMNH 2013-07-0563 (Figure 6) is roughly rectangular in shape, preserving the original margin of the shell on one side and disarticulated along sutural margins along the other three. It measures 109.36 mm in its longest dimension by 94.97 mm perpendicular to that. The bone is deformed, with significant fracturing and flattening that has been stabilized with adhesives (Figure 6A). The entirety of the surficial shell, exposed on both sides of the fragment, is covered with numerous small, round depressions that cluster around 2 mm in diameter. These structures are mostly randomly distributed, with a few regions that exhibit localized patterning, either as rings, linear chains of depressions, or merging patches of overlapping structures (Figure 8C).

DMNH 2013-07-0563 exhibits irregularly spaced shallow pits along its surface and small internal hollows only visible in CT reconstructions. These small internal hollows are close to the exterior of the fossil but appear unconnected to any nearby pit or the bone surface. Outlines suggesting bone compression are nonexistent in this sample (Figure 6B-6E). Pit depth appears to vary, with some pits being shallower than others (Table 3).

DISCUSSION

Differentiating between advanced shell disease, which is characterized by the etching or biological erosion of cortical bone and the exposure and further degradation of the underlying trabecular bone (Zonneveld and Bartels, 2022), and more penetrative bite marks, punctures, and furrows that pierce bone surfaces and are associated with extensive crushing and compression damage (Binford, 1981), is possible under low to no magnification. These two types of bone damage are not particularly convergent, and represent the majority of previously published examples (e.g., Hutchinson and Frye, 2001; Fuentes, 2003; Karl and Tichy, 2004; Mead et al., 2006; Steadman et al., 2007; Milàn et al., 2011; Evgen et al., 2012; Noto et al.,

2012; Morgan and Albury, 2013; Botfalvai et al., 2014, 2015; Hastings et al., 2015; Cerda et al., 2016; de Valais et al., 2020).

However, less advanced examples of shell disease and less penetrative bite marks can produce highly convergent patterns of surficial bone damage. Both are expressed as rounded depressions, often with a relatively smooth interior. The compression and fracturing characteristic of bite marks can be subtle in shallower traces, even under low magnification, making equifinality an issue when attempting to differentiate these two types of bone damage in hand sample (Hutchinson and Frye, 2001; Chamberlain and Corsini, 2006-2007; Corsini and Chamberlain, 2009; Rothschild et al., 2013).

Fortunately, the mechanism by which these two pathologies form is highly divergent, and this is expressed more clearly in the internal structure of bones affected by each type of damage. Bite marks are caused by impact trauma and compressive forces indenting the surface of the bone (Figure 8B and 8D). Under minimal compression, the layer of dense cortical bone is pressed down into the underlying, less dense trabecular bone. In CT scans, this is expressed as a layer of dense bone of fairly uniform thickness that tracks the surface of the affected element, following the internal morphology of a bite mark. With heightened forces, the layer of cortical bone under a bite mark can become thicker with a higher density as the affected bone is compacted under the impacting tooth (Figures 1, 2, and 3).

Shell disease is driven by an immune response to an irritant or infection between the bone of the carapace or plastron of a turtle and the overlying scutes (Hunt, 1957; Garner et al., 1997; Hutchinson and Frye, 2001; Jacobson, 2007; Rothschild et al., 2013). There are no associated compressive forces involved in this type of damage, and instead, shell disease etches into the surface of the bone, cutting across the cortical bone. This leaves the surface of the cortical to trabecular bone transition largely unaffected, unless the shell disease progresses to a point that it completely penetrates the outermost cortical layer, exposing the trabecular bone beneath (Figure 8A and 8C). In CT scans, this is expressed as an undeformed layer of dense cortical bone, marked by eroded depressions, some of which are further associated with bubble-shaped voids under the surface of the pathology (Figures 4, 5, and 6).

CONCLUSIONS

Bone surface modifications and pathologies can each provide rich paleoecological insights into the conditions surrounding the life, death, and burial of fossil organisms. However, those data only become accessible when paleontologists are able to differentiate the various types of bone damage. Unfortunately, some processes can result in convergent patterns of expression. This type of equifinality can result in misidentification and misinterpretation of damage patterns on bones.

Though advanced shell disease and deeply penetrative tooth marks are morphologically distinct, more subtle damage caused by these two very different processes can result in convergent surficial expressions. This has led to concerns surrounding paleontologists' ability to positively identify the sources of rounded depressions in fossil turtle shells (e.g., Hutchinson and Frye, 2001; Chamberlain and Corsini, 2006-2007; Corsini and Chamberlain, 2009; Rothschild et al., 2013). However, the application of non-destructive CT methods provides a pathway for differentiating these two types of bone damage. Internal visualization of modern and fossil examples of damaged turtle shells reveals that the compressive forces associated with bite marks result in disparate bone textures from the erosional progression that characterizes shell disease formation.

ACKNOWLEDGEMENTS

The Perot Museum of Nature and Science, UT Anthropology, and the St. Augustine Alligator Farm and Zoological Park provided access to specimens. The National Science Foundation DUE-IUSE GP-IMPACT grant #1600376 to L. McKay and S. Horn, The National Geographic Society Conservation Trust grant #C325-16 to C. Noto, UT Earth and Planetary Sciences, VT Department of Geosciences, and donors through Experiment.com provided funding. CT scans were performed by B. Wynd and J. Gladman at SMIF. This manuscript was improved with the helpful feedback of S. deValais, G. Botfalvai, two anonymous reviewers, and our editor, R. Felice.

REFERENCES

Adams, T.L., Polcyn, M.J., Mateus, O., Winkler, D.A., and Jacobs, L.L. 2011. First occurrence of the long-snouted crocodyliform *Terminonaris* (Pholidosauridae) from the Woodbine Formation (Cenomanian) of Texas. Journal of Vertebrate Paleontology, 31:712-716 https://doi.org/10.1080/02724634.2011.572938

Adams, T.L., Noto, C.R., and Drumheller, S. 2017. A large neosuchian crocodyliform from the Upper Cretaceous (Cenomanian) Woodbine Formation of North Texas. Journal of Vertebrate Paleontology, 37:e1349776. https://doi.org/10.1080/02724634.2017.1349776

Adrian, B., Smith, H.F., Noto, C.R., and Grossman, A. 2019. A new baenid, *"Trinitichelys" maini* sp. nov., and other fossil turtles from the Upper Cretaceous Arlington Archosaur Site (Woodbine Formation, Cenomanian), Texas, USA. Palaeontologia Electronica, 22.3.81. https://doi.org/10.26879/1001

Ambrose, W.A., Hentz, T.F., Bonnaffe, F., Loucks, R.G., Brown Jr., L.F., Wang, F.P., and Potter, E.C. 2009. Sequence-stratigraphic controls on complex reservoir architecture of highstand fluvial-dominated deltaic and lowstand valley-fill deposits in the Upper Cretaceous (Cenomanian) Woodbine Group, East Texas field: Regional and local perspectives: AAPG Bulletin, 93:231-269. https://doi.org/10.1306/09180808053

Augustin, F.J., Matzke, A.T., Csiki-Sava, Z., and Pfretzschner, H.U. 2019. Bioerosion on vertebrate remains from the Upper Cretaceous of the Haţeg Basin, Romania and its taphonomic implications. Palaeogeography, Palaeoclimatology, Palaeoecology, 534:109318. https://doi.org/10.1016/j.palaeo.2019.109318

Barnes, V.E. 1972. Geological Atlas of Texas, Dallas Sheet. Bureau of Economic Geology, University of Texas at Austin.

Behrensmeyer, A.K., Gordon, K.D., and Yanagi, G.T. 1986. Trampling as a cause of bone surface damage and pseudo-cutmarks. Nature, 319:768-771. https://doi.org/10.1038/319768a0

Binford, L.R. 1981. Bones: Ancient Men and Modern Myths. Academic Press, New York. https://doi.org/10.1016/C2013-0-07180-0

Botfalvai, G., Prondvai, E., and Ősi, A. 2014. Inferred bite marks on a Late Cretaceous (Santonian) bothremydid turtle and a hylaeochampsid crocodilian from Hungary. Cretaceous Research, 50:304-317. https://doi.org/10.1016/j.cretres.2014.05.006

Botfalvai, G., Ősi, A., and Mindszenty, A. 2015. Taphonomic and paleoecologic investigations of the Late Cretaceous (Santonian) Iharkút vertebrate assemblage (Bakony Mts, northwestern Hungary). Palaeogeography, Palaeoclimatology, Palaeoecology, 417:379-405. https://doi.org/10.1016/j.palaeo.2014.09.032

Boyd, C.A., Drumheller, S.K., and Gates, T.A. 2013. Crocodyliform feeding traces on juvenile ornithischian dinosaurs from the Upper Cretaceous (Campanian) Kaiparowits Formation, Utah. PloS ONE, 8:e57605. https://doi.org/10.1371/journal.pone.0057605

Cerda, I.A., Sterli, J., and Scheyer, T.M. 2016. Bone shell microstructure of *Condorchelys antiqua* Sterli, 2008, a stem turtle from the Jurassic of Patagonia. Comptes Rendus Palevol, 15:128-141. https://doi.org/10.1016/j.crpv.2015.01.004

Chamberlain, H. and Corsini, J. 2006-2007. Characterization of a modern turtle deathsite and comparison with a paleo-deathsite. Eastern Oregon Science Journal, 20:14-19.

Corsini, J.A. and Chamberlain, H. 2009. Characterization of modern turtle death sites for comparison with late Eocene and early Oligocene turtle sites. The American Midland Naturalist, 161:96-109. https://doi.org/10.1674/0003-0031-161.1.96

D'Amore, D.C. and Blumensehine, R.J. 2009. Komodo monitor (*Varanus komodoensis*) feeding behavior and dental function reflected through tooth marks on bone surfaces, and the application to ziphodont paleobiology. Paleobiology, 35:525-552. https://doi.org/10.1666/0094-8373-35.4.525

de Valais, S., Díaz-Martínez, I., Citton, P., Maniel, I., and de la Fuente, M. 2020. A predation attempt in a Late Cretaceous pleurodire turtle from Patagonia. Cretaceous Research, 107:104290. https://doi.org/10.1016/j.cretres.2019.104290

Domínguez-Solera, S.D. and Domínguez-Rodrigo, M. 2009. A taphonomic study of bone modification and of tooth-mark patterns on long limb bone portions by suids. International Journal of Osteoarchaeology, 19:345-363. https://doi.org/10.1002/oa.987

Donovan, A.D., Gardner, R.D., Pramudito, A., Staerker, T.S., Wehner, M., Corbett, M.J., Lundquist, J.J., Romero, A.M., Henry, L.C., and Rotzien, J.R. 2015. Chronostratigraphic relationships of the Woodbine and Eagle Ford Groups across Texas. GCAGS Journal, 4:67-87.

Drumheller, S.K. and Brochu, C.A. 2014. A diagnosis of *Alligator mississippiensis* bite marks with comparisons to existing crocodylian datasets. Ichnos, 21:131-146. https://doi.org/10.1080/10420940.2014.909353

Drumheller, S.K., Stocker, M.R., and Nesbitt, S.J. 2014. Direct evidence of trophic interactions among apex predators in the Late Triassic of western North America. Naturwissenschaften, 101:975-987. https://doi.org/10.1007/s00114-014-1238-3

Drumheller, S.K. and Brochu, C.A. 2016. Phylogenetic taphonomy: a statistical and phylogenetic approach for exploring taphonomic patterns in the fossil record using crocodylians. Palaios, 31:463-478. https://doi.org/10.2110/palo.2016.030

Drumheller, S.K., McHugh, J.B., Kane, M., Riedel, A., and D'Amore, D.C. 2020. High frequencies of theropod bite marks provide evidence for feeding, scavenging, and possible cannibalism in a stressed Late Jurassic ecosystem. PLoS ONE, 15:e0233115. https://doi.org/10.1371/journal.pone.0233115.

Drumheller, S.K., Adams, T.L., Maddox, H., and Noto, C.R. 2021. Expanded Sampling Across Ontogeny in *Deltasuchus motherali* (Neosuchia, Crocodyliformes): Revealing Ecomorphological Niche Partitioning and Appalachian Endemism in Cenomanian Crocodyliforms. Elements of Paleontology: 1-67. https://doi.org/10.1017/9781009042024

Emerson, B.L., Emerson, J.H., Akers, R.E., and Akers, T.J. 1994. Texas Cretaceous ammonites and nautiloids. Houston Gem & Mineral Society, Houston, Texas.

Erickson, G.M., Gignac, P.M., Steppan, S.J., Lappin, A.K., Vliet, K.A., Brueggen, J.D., Inouye, B.D., Kledzik, D., and Webb, G.J.W. 2012. Insights into the ecology and evolutionary success of crocodilians revealed through bite-force and tooth-pressure experimentation. PLoS ONE, 7:e31781. https://doi.org/10.1371/journal.pone.0031781

Erickson, G.M., Gignac, P.M., Lappin, A.K., Vliet, K.A., Brueggen, J.D., and Webb, G.J.W. 2014. A comparative analysis of ontogenetic bite-force scaling among Crocodylia. Journal of Zoology, 292:48-55. https://doi.org/10.1111/jzo.12081

Звонок, Є., Удовиченко, М., & Братішко, А., 2012. Misceznakhodzhennya eocenovykh khrebetnykh Ikove (Luhanska oblast, Ukraina): ecologo-taphonomichnyi analiz. Paleontologichnyi zbirnyk and Paleontological Review, 44:107-122. (In Ukrainian and English)

Farlow, J.O. and Holtz, T.R. 2012. The fossil record of predation in dinosaurs. The Paleontological Society Papers, 8:251-266. https://doi.org/10.1017/S108933260000111X

Fiorillo, A.R. 1991. Prey bone utilization by predatory dinosaurs. Palaeogeography, Palaeoclimatology Palaeoecology, 88:157-166. https://doi.org/10.1016/0031-0182(91)90062-V

Fuentes, E.J. 2003. Predación crocodiliana a quelonios: un *Neochelys* (Pelomedusidae), del Eoceno de Zamora, lisiado por un *Asiatosuchus* [Crocodylian predation on chelonians: a *Neochelys* (Pelomedusidea) from the Eocene of Zamora, crippled by an *Asiatosuchus*. Studia Geologica Salmanticensia, 39:11-23.

Garner, M.M., Herrington, R., Howerth, E.W., Homer, B.L., Nettles, V.F., Isaza, R., Shotts, Jr., E.B., and Jacobson, E.R. 1997. Shell disease in river cooters (*Pseudemys concinna*) and yellow–bellied turtles (*Trachemys scripta*) in a Georgia (USA) lake. Journal of Wildlife Diseases, 33:78-86. https://doi.org/10.7589/0090-3558-33.1.78

Gignac, P.M. and Erickson, G.M. 2016. Ontogenetic bite-force modeling of *Alligator mississippiensis*: implications for dietary transitions in a large-bodied vertebrate and the evolution of crocodylian feeding. Journal of Zoology, 299:229-238. https://doi.org/10.1111/jzo.12349

Gradstein, F.M., Ogg, J.G., and Smith, A.G. (eds.), 2004. A Geologic Time Scale 2004. Cambridge University Press, Cambridge, UK.

Hamm, C.A., Hampe, O., Schwarz, D., Witzmann, F., Makovicky, P.J., Brochu, C.A., Reiter, R., and Asbach, P. 2020. A comprehensive diagnostic approach combining phylogenetic disease bracketing and CT imaging reveals osteomyelitis in a *Tyrannosaurus rex*. Scientific Reports, 10:1-16. https://doi.org/10.1038/s41598-020-75731-0

Hastings, A.K., Bloch, J.I., and Jaramillo, C.A. 2015. A new blunt-snouted dyrosaurid, *Anthracosuchus balrogus* gen. et sp. nov. (Crocodylomorpha, Mesoeucrocodylia), from the Palaeocene of Colombia. Historical Biology, 27:998-1020. https://doi.org/10.1080/08912963.2014.918968

Haynes, G. 1983. A guide for differentiating mammalian carnivore taxa responsible for gnaw damage to herbivore long bones. Paleobiology, 9:164-172. https://doi.org/10.1017/S0094837300007545

Hone, D.W.E. and Rauhut, O.W. 2010. Feeding behavior and bone utilization by theropod dinosaurs. Lethaia, 43:232-244. https://doi.org/10.1111/j.1502-3931.2009.00187.x

Hunt, T.J. 1957. Notes on diseases and mortality in testudines. Herpetologica, 13:19-23.

Hutchison, J.H. and Frye, F.L. 2001. Evidence of pathology in early Cenozoic turtles. PaleoBios, 21:12-19.

Jacobson, E.R. 2007. Infectious Diseases and Pathology of Reptiles: Color Atlas and Text. CRC Press, Boca Raton, Louisiana. https://doi.org/10.1201/9781420004038

Karl, H.V. and Tichy, G. 2004. The structure of fossil teeth of chelonophagous crocodiles (Diapsida: Crocodylia). Studia Geologica Salmanticensia, 40:115-124.

Katsura, Y. 2004. Paleopathology of *Toyotamaphimeia machikanensis* (Diapsida, Crocodylia) from the middle Pleistocene of central Japan. Historical Biology, 16:93-97. https://doi.org/10.1080/08912963400015041

Kennedy, W.J. and Cobba, W.A. 1990. Cenomanian ammonite faunas from the Woodbine Formation and lower part of the Eagle Ford Group, Texas. Palaeontology, 33:75-154.

Lovich, J.E., Gotte, S.W., Ernst, C.H., Harshbarger, J.C., Laemmerzahl, A.F., and Gibbons, J.W. 1996. Prevalence and histopathology of shell disease in turtles from Lake Blackshear, Georgia. Journal of Wildlife Diseases, 32, 259-265. https://doi.org/10.7589/0090-3558-32.2.259

Mackness, B.S., Cooper, J.E., Wilkinson, C.E.C., and Wilkinson, D. 2010. Palaeopathology of a crocodile femur from the Pliocene of eastern Australia. Alcheringa, 34:515-521. https://doi.org/10.1080/03115511003793512

McHugh, J.B., Drumheller, S.K., Riedel, A., and Kane, M. 2020. Decomposition of dinosaurian remains inferred by invertebrate traces on vertebrate bone reveal new insights into Late Jurassic ecology, decay, and climate in western Colorado. PeerJ, 8:e9510. https://doi.org/10.7717/peerj.9510

Mead, J.I., Cubero, R., Zamora, A.L.V., Swift, S.L., Laurito, C., and Gómez, L.D. 2006. Plio-Pleistocene *Crocodylus* (Crocodylia) from southwestern Costa Rica. Studies on Neotropical Fauna and Environment, 41:1-7. https://doi.org/10.1080/01650520500309917

Milàn, J., Lindow, B.E., and Lauridsen, B.W. 2011. Bite traces in a turtle carapace fragment from the middle Danian (Lower Paleocene) bryozoan limestone, Faxe, Denmark. Bulletin of the Geological Society of Denmark, 59: 61-67.

Morgan, G.S. and Albury, N.A. 2013. The Cuban crocodile (*Crocodylus rhombifer*) from late Quaternary fossil deposits in the Bahamas and Cayman Islands. Bulletin of the Florida Museum of Natural History, 52:161-236.

Njau, J.K. and Blumenschine, R.J. 2006. A diagnosis of crocodile feeding traces on larger mammal bone, with fossil examples from the Plio-Pleistocene Olduvai Basin, Tanzania. Journal of Human Evolution, 50:142-162. https://doi.org/10.1016/j.jhevol.2005.08.008

Njau, J. and Gilbert, H. 2016. Standardizing terms for crocodile-induced bite marks on bone surfaces in light of the frequent bone modification equifinality found to result from crocodile feeding behavior, stone tool modification, and trampling. FOROST (Forensic Osteology) Occasional Publications, 3:1-13.

Noto, C.R., Main, D.J., and Drumheller, S.K. 2012. Feeding traces and paleobiology of a Cretaceous (Cenomanian) crocodyliform: example from the Woodbine Formation of Texas. Palaios, 27:105-115. https://doi.org/10.2110/palo.2011.p11-052r

Noto, C.R., Drumheller, S.K., Adams, T.L., and Turner, A.H. 2020. An enigmatic small neosuchian crocodyliform from the Woodbine Formation of Texas. The Anatomical Record, 303, 801-812. https://doi.org/10.1002/ar.24174

Paik, I.S., Kim, H.J., Lim, J.D., Huh, M., and Lee, H.I. 2011. Diverse tooth marks on an adult sauropod bone from the Early Cretaceous, Korea: Implications in feeding behavior of theropod dinosaurs. Palaeogeography, Palaeoclimatology, Palaeoecology, 209:342-346. https://doi.org/10.1016/j.palaeo.2011.07.002

Rega, E.A., Noriega, K., Sumida, S.S., Huttenlocker, A., Lee, A., and Kennedy, B. 2012. Healed fractures in the neural spines of an associated skeleton of *Dimetrodon*: implications for dorsal sail morphology and function. Fieldiana Life and Earth Sciences, 2012(5):104-111. https://doi.org/10.3158/2158-5520-5.1.104

Rogers, R.R., Krause, D.W., and Curry Rogers, K. 2003. Cannibalism in the Madagascan dinosaur *Majungatholus atopus*. Nature, 422:515-518. https://doi.org/10.1038/nature01532

Rothschild, B.M., Schultze, H.P., and Pellegrini, R. 2013. Osseous and other hard tissue pathologies in turtles and abnormalities of mineral deposition, p. 501-534. In Brinkman, D., Holroyd, P., and Gardner, J. (eds.), Morphology and Evolution of Turtles. Vertebrate Paleobiology and Paleoanthropology. Springer, Dordrecht. https://doi.org/10.1007/978-94-007-4309-0_27

Saneyoshi, M., Watabe, M., Suzuki, S., and Tsogthbaatar, K. 2011. Trace fossils on dinosaur bones from Upper Cretaceous eolian deposits in Mongolia: Taphonomic interpretations of paleoecosystems in ancient desert environments. Palaeogeography, Palaeoclimatology, Palaeoecology, 311:38-47. https://doi.org/10.1016/j.palaeo.2011.07.024

Scheyer, T.M. 2009. Conserved bone microstructure in the shells of long-necked and short-necked chelid turtles (Testudinata, Pleurodira). Fossil Record, 12:47-57. https://doi.org/10.1002/mmng.200800009

Steadman, D.W., Franz, R., Morgan, G.S., Albury, N.A., Kakuk, B., Broad, K., Franz, S.E., Tinker, K., Pateman, M.P., Lott, T.A., Jarzen, D.M., and Dilcher, D.L. 2007. Exceptionally well preserved late Quaternary plant and vertebrate fossils from a blue hole on Abaco, The Bahamas. Proceedings of the National Academy of Sciences 104:19897-19902. https://doi.org/10.1073/pnas.0709572104

Strganac, C. 2015. Field Trip Overview in Early and Mid-Cretaceous Archosaur Localities of North-Central Texas. In Noto, C.R. (ed.), Fieldtrip Guidebook 2–4, Society of Vertebrate Paleontology Annual Meeting.

Tanke, D. and Currie, P.J. 1998. Head-biting behavior in theropod dinosaurs: paleopathological evidence. Gaia, 15:167-184. https://doi.org/10.7939/R34T6FJ1P

Zonneveld, J.P., Bartels, W.S., Gunnell, G.F., and McHugh, L.P., 2015. Borings in early Eocene turtle shell from the Wasatch Formation, South Pass, Wyoming. Journal of Paleontology, 89:802-820. https://doi.org/10.1017/jpa.2015.61

Zonneveld, J.P. and Bartels, W.S. 2022. The occurrence of bone modification features in the carapace and plastron of the extant red-eared slides *Trachemys scripta elegans* (Wied-Neuwied, 1839): Implications for paleoecological analyses of fossil turtle assemblages. Palaios, 37:499-519. https://doi.org/10.2110/palo.2022.018

Zonneveld, J.P., Fiorillo, A.R., Hasiotis, S., and Gingras, M.K. 2022. Tooth marks, gnaw marks, claw-marks, bite marks, scratch marks, etc: Terminology in ichnology. Ichnos, 2022, 29: 93-101. https://doi.org/10.1080/10420940.2022.2058937